Athermalization of the Lasing Wavelength in Vertical-Cavity Surface-Emitting Lasers

N.B. When citing this work, cite the original published paper.

(article starts on next page)

Athermalization of the Lasing Wavelength in Vertical-Cavity Surface-Emitting Lasers

Lars Persson,* Filip Hjort, Giulia Cardinali, Johannes Enslin, Tim Kolbe, Tim Wernicke, Michael Kneissl, Joachim Ciers, and Åsa Haglund*

A concept for vertical-cavity surface-emitting lasers (VCSELs) is proposed and demonstrated to obtain a lasing wavelength with unprecedented temperature stability. The concept is based on incorporating a dielectric material with a negative thermo-optic coefficient, dn/dT, in the distributed Bragg reflectors (DBRs) to compensate the positive dn/dT of the semiconductor cavity. In a short cavity, the optical field has a significant overlap with the DBRs, and the redshift of the lasing wavelength caused by the semiconductor cavity can be compensated by the negative dn/dT of the DBRs. Here, proof of this concept is presented for optically-pumped VCSELs emitting at 310 nm, demonstrating a lasing wavelength that even blueshifts by less than 0.1 nm over an 80 °C range with a maximum slope of -3.4 pm K^{-1}. This is to be compared with a redshift of 1–1.5 nm over the same temperature range reported for III-nitride blue-emitting VCSELs. Furthermore, this method can also be implemented in VCSELs with longer cavity lengths by including a dielectric layer between the semiconductor and the DBR. The approach used here to obtain a temperature-stable lasing wavelength is generic and can therefore be applied to VCSELs in all material systems and lasing wavelengths.

1. Introduction

Lasers in applications such as gas sensing,[1] atomic clocks,[2] and fiber-optical communication systems[3,4] would greatly benefit from having a temperature-stable lasing wavelength. For these wavelength-sensitive applications, vertical-cavity surface-emitting lasers (VCSELs) are the preferred laser type, since they have a lasing wavelength which is set by the cavity resonance rather than the gain peak and the cavity resonance shifts less with increasing temperature.[5]

Even though VCSELs are much more temperature-stable than other lasers, the lasing wavelength of most VCSELs redshifts with increasing temperature.[6] The wavelength shift with temperature for III-nitride VCSELs has so far only been reported for blue-emitting VCSELs and typical values lie within the range of 12–18.5 pm K^{-1}.[7–11] The reason for this redshift is that semiconductor materials have a positive thermo-optic coefficient, dn/dT, in their transparency window, and an increase of the refractive index with temperature increases the optical thickness of the cavity.

Current solutions to avoid the inherent redshift caused by the semiconductor material include temperature-stabilizing feedback loops and power-hungry thermo-electric coolers.[12] However, these solutions can be both expensive and bulky and an inherently temperature-stable VCSEL would be desired.

This could be achieved by the inclusion of materials with a negative dn/dT in the cavity to compensate the redshift caused by the semiconductor, a strategy often used to achieve athermal passive components such as ring resonators and waveguides.[13–16] The sign of a material's dn/dT is set by two competing processes.[17] With an increased temperature, thermal expansion reduces the material density, lowering the refractive index. At the same time, the atomic bonds weaken, leading to a higher electron polarizability of the material and an increased refractive index. If the first effect dominates, the material will have a negative dn/dT. This can for example occur in the dielectrics SiO_2,[18] TiO_2,[3,18,19] and Ta_2O_5.[3] The dn/dT of these dielectric materials heavily depends on the deposition method and parameters. It was recently proposed theoretically to use TiO_2 as a passive cavity, and as one of the two materials in the distributed Bragg reflector (DBR) in a VCSEL which has the active region within the epitaxial DBR.[3] However, this leads to a three-fold reduction of the confinement factor when compared to an active region placed in the cavity between the DBRs.[3] To the best of our knowledge, this proposal has not been experimentally verified.

L. Persson, F. Hjort, J. Ciers, Å. Haglund
Department of Microtechnology and Nanoscience
Chalmers University of Technology
Gothenburg 41296, Sweden
E-mail: lars.persson@chalmers.se; asa.haglund@chalmers.se
G. Cardinali, J. Enslin, T. Wernicke, M. Kneissl
Institute of Solid State Physics
Technische Universität Berlin
10623 Berlin, Germany
T. Kolbe, M. Kneissl
Ferdinand-Braun-Institut
12489 Berlin, Germany

In this paper, we propose an alternative design for a temperature-stable laser and demonstrate this both experimentally and theoretically for a 2.5λ AlGaN-based UV VCSEL with two dielectric DBRs. Our approach is based on using a standard semiconductor cavity with quantum wells (QWs) and a dielectric material with a negative dn/dT, in our case HfO_2. In a short cavity, implementing HfO_2 in the dielectric DBRs is sufficient to obtain a temperature-stable lasing wavelength. When using longer cavities, that is, to reduce the thermal resistance, then it is necessary to also place HfO_2 between the semiconductor cavity and the dielectric DBR to achieve full compensation. These approaches are applicable to VCSELs emitting at any wavelength as long as materials with negative dn/dT can be incorporated in the cavity or DBRs.

2. Analytical Design Formula for Athermal Resonance Wavelength

The redshift observed in most III-nitride VCSELs can be well estimated by considering the temperature dependence of the longitudinal resonance wavelength of a Fabry-Perot cavity[5]

$$\frac{d\lambda_{FP}}{dT} = \frac{\lambda_0}{\bar{n}_c}\frac{d\bar{n}_c}{dT}, \tag{1}$$

where $\bar{n}_c$ is the average refractive index of the cavity. In Equation (1), the thermal expansion of the cavity as well as the wavelength dispersion are neglected. In spite of this, Equation (1) produces a value of ≈ 15.7 pm K^{-1}, when only considering a GaN cavity with $d\bar{n}_c/dT \approx 7.9 \times 10^{-5}$ K^{-1}, which is close to the experimentally reported values for III-nitride cavities of 12–18.5 pm K^{-1}.[7–11] Even though Equation (1) reproduces the redshift of most III-nitride VCSELs, it still doesn't capture important subtleties within the VCSEL structure, such as mirror composition and cavity length.

The effect of two DBRs on the wavelength of the longitudinal modes, λ_m, is twofold: first, an effective cavity length, $L_{eff} = L_c + L_{pt} + L_{pb}$, where $L_{pt/b}$ is the phase penetration depth of the top (t) and bottom (b) DBR,[5] has to be accounted for, and second, the detuning between the longitudinal mode and the center wavelengths of the DBRs, $\lambda_{t/b}$, has to be considered,[5,21] which results in

$$\lambda_m = \frac{2\bar{n}_c L_{eff}}{m + 2\bar{n}_c(L_{pt}/\lambda_t + L_{pb}/\lambda_b)}, \tag{2}$$

where m is the mode number (a positive integer). From Equation (2), it is possible to derive an expression for the longitudinal mode shift with temperature, see Section S1 (Supporting Information). If the top and bottom DBRs are identical ($L_{pt} = L_{pb} = L_p$ and $\lambda_t = \lambda_b = \lambda_{DBR}$) this shift is given by

$$\frac{d\lambda}{dT} = \frac{d\lambda_{FP}/dT + (2L_{p0}/L_c)d\lambda_{DBR}/dT}{1 + 2L_{p0}/L_c}. \tag{3}$$

where the subindex 0 indicates values at room temperature, $d\lambda_{FP}/dT$ is given by Equation (1), $d\lambda_{DBR}/dT \approx 2(d_L dn_L/dT + d_H dn_H/dT)$ is the shift of the center wavelength of the DBRs

with temperature,[5] and subindex L/H refers to the low/high refractive index materials in the DBR. As can be seen in Equation (3), there are in principle two ways in which a temperature-stable resonance can be obtained, both relying on the use of materials with a negative dn/dT. First, if the cavity of the VCSEL is short, the penetration depth of the optical field into the DBRs relative to the total cavity length, L_{p0}/L_c, becomes significant and the resonance shift of the DBR center wavelength must be considered when determining the overall shift of the longitudinal cavity mode. By choosing dielectric materials with negative dn/dT so that $d\lambda_{DBR}/dT < 0$, the positive redshift caused by the semiconductor cavity, $d\lambda_{FP}/dT$, can be compensated to produce a temperature-stable resonance wavelength, $d\lambda/dT \approx 0$. Second, if the cavity is long, then the penetration depth becomes insignificant in relation to the cavity length, $L_{p0}/L_c \approx 0$, making the influence of the DBRs negligible. In this case, it is still possible to produce $d\lambda/dT \approx 0$ by incorporating a thick dielectric spacer layer with a negative dn/dT within the cavity to compensate for the positive dn/dT of the semiconductor, so that $d\lambda/dT \approx d\lambda_{FP}/dT \approx 0$.

3. UVB VCSEL Design and Characterization

We demonstrate a temperature-stable lasing wavelength from a ultraviolet B (UVB)-emitting (280-320 nm) VCSEL using the first approach with a short AlGaN cavity length and two dielectric DBRs, with one dielectric material having a negative dn/dT. The devices we investigate here are optically pumped UVB-VCSELs emitting around 310 nm, which were recently demonstrated by our groups.[20] The device layout and the cavity structure, together with the standing optical field within the cavity, are shown in **Figure 1**. The $Al_{0.6}Ga_{0.4}N$ cavity has an optical thickness of 2.5λ. The active region consists of three 2-nm-thick $Al_{0.2}Ga_{0.8}N$ quantum-wells (QWs) with 5-nm-thick $Al_{0.5}Ga_{0.5}N$ barriers. The cavity is defined by two dielectric HfO_2/SiO_2 DBRs, realized by a substrate removal technique using electrochemical etching of AlGaN sacrificial layers.[22] A 10-nm-thick HfO_2 spacer layer is added between the cavity and bottom DBR in order to better align the QWs with the antinode of the optical field and to control the resonance wavelength.[23] It should be noted that the short cavity length leads to a significant part of the optical intensity distribution overlapping with the DBRs, which have a negative dn/dT, as can be seen in Figure 1b. The dn/dT for the materials used in this work, SiO_2, HfO_2, and $Al_xGa_{1-x}N$ are shown in **Figure 2** for a wavelength of 310 nm (close to the lasing wavelength of the fabricated VCSELs). More information about the measurement and modeling of $n(T)$ can be found in the Experimental Section.

Under optical pumping these VCSELs lase at a few different wavelengths simultaneously due to filamentation.[20] However, all of these laser lines shift similarly with temperature as shown in Section S3 (Supporting Information). In **Figure 3**, the measured optical spectrum as a function of substrate temperature is shown for one of these lasing lines for a pump power of 25 % above the threshold pump power density of 2 MW cm^{-2} at room temperature. Over a temperature range from 22 °C to 80 °C, the wavelength shifts by less than 0.1 nm. The maximum slope of the shift is −3.4 pm K^{-1} between 30 and 50 °C. This wavelength shift is to be compared with values for blue-emitting VCSELs, which are positive and range from 12 to 18.5 pm K^{-1}, that is, shifting by 0.7–1.1 nm in the same temperature range.[7–11] This means

ADVANCED
SCIENCE NEWS
www.advancedsciencenews.com

LASER
& PHOTONICS
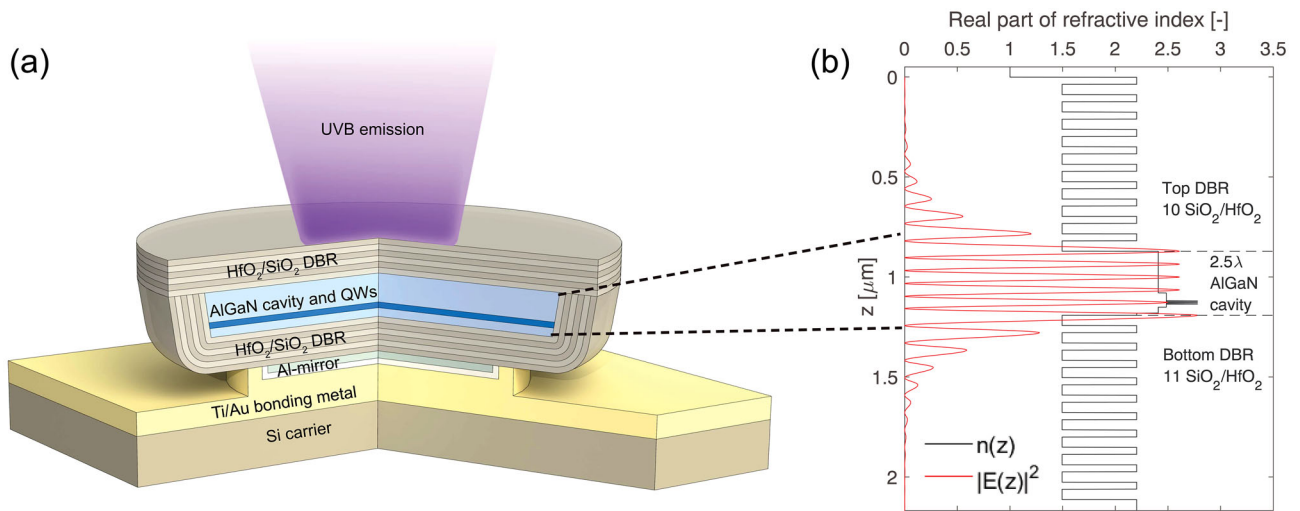REVIEWS

www.lpr-journal.org

Figure 1. a) Schematic structure of the UVB VCSEL. Figure adopted from Ref. [20]. b) Optical field intensity (red) and the refractive index (black) along the vertical direction of the 2.5λ cavity.
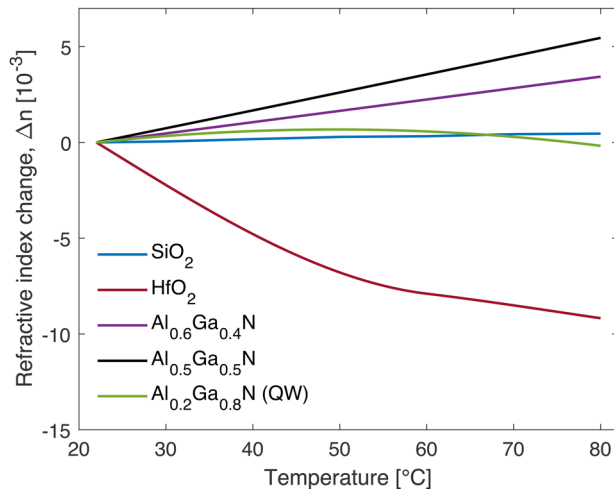

Figure 2. Refractive index change with temperature, $\Delta n(T)$, at 310 nm. More details can be found in Experimental Section.
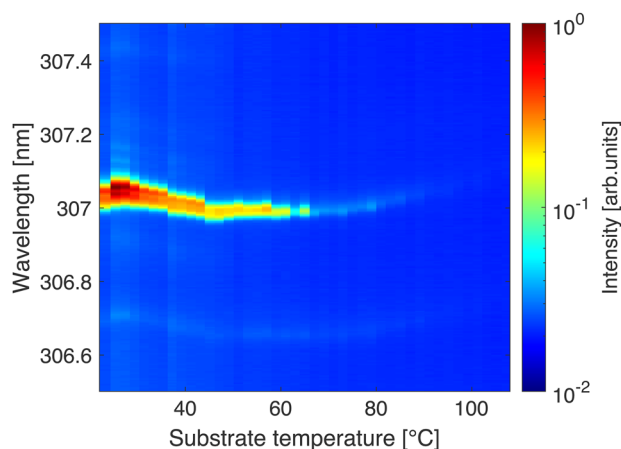

Figure 3. Emission spectrum of the UVB VCSEL for different substrate temperatures.

that the measured values of the wavelength shift is more than a factor 7 smaller than reported values.[7–11] Thus, we show that it is possible not only to reduce the expected redshift from a VCSEL due to its semiconductor cavity, but even overcompensate it and demonstrate a blueshift with increasing temperature. In the following section, we will discuss the quantitative agreement of the wavelength shift based on Equation (3) using the measured refractive index data.

4. Simulated Temperature Dependence of the Resonance Wavelength

In order to verify and understand the athermal emission wavelength concept implemented for the UVB VCSEL, the resonance wavelength shift as a function of temperature, $\Delta\lambda(T)$, was calculated by Equation (2) and simulated using the effective index method (EIM).[24] The results are displayed in **Figure 4**. Note that the changing standing wave due to temperature-induced refractive index changes is taken into account in the EIM simulations. If the influence of dn/dT of the dielectric materials in the DBRs is omitted, that is, dn/dT is set to zero, the resonance wavelength redshifts linearly with increasing temperature at a rate of 4.3 pm K^{-1}, see Figure 4a. In order to mimic some of the effects of an epitaxial mirror, dn/dT of the dielectric materials is set to the value of Al$_{0.6}$Ga$_{0.4}$N, 5.9×10^{-5} K^{-1}. This results in an even larger linear increase of the resonance wavelength, 6.9 pm K^{-1}, which is in good agreement with Equation (1). However, by including the measured dn/dT for HfO$_2$, the behavior changes drastically. The resonance wavelength now shifts minimally between room temperature and 50 °C and reproduces the athermal behavior that was observed experimentally. Thus, the dn/dT of the dielectric DBRs greatly influences the thermal shift of the resonance wavelength. This is also reflected by Equation (2) as seen in Figure 4a. The refractive index is not only affected by temperature, but also by carrier concentration which increases at higher temperatures due to an increased threshold. The impact of the carrier concentration on $\Delta\lambda$ is small in comparison with the effect of HfO$_2$ since the QW thickness constitutes a very small fraction of the overall
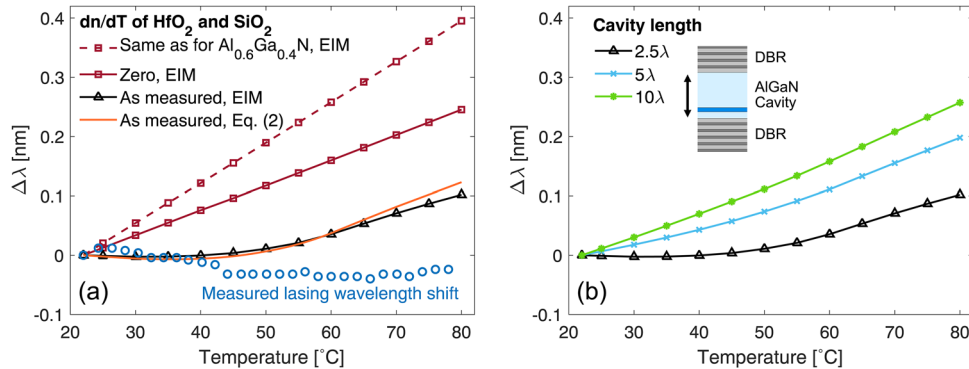
Figure 4. Simulated wavelength shift as a function of temperature, $\Delta\lambda(T)$, of the UVB VCSEL. a) Illustrating the impact of dn/dT of HfO_2 on $\Delta\lambda(T)$ by using the measured value for HfO_2 of $dn/dT = -2.1 \times 10^{-4}$ K^{-1} and for SiO_2 of $dn/dT = 8.1 \times 10^{-6}$ K^{-1} (black triangles and solid orange line) and comparing it to two artificial cases where dn/dT of HfO_2 and SiO_2 is set to that of $Al_{0.6}Ga_{0.4}N$, 5.9×10^{-5} K^{-1} (dashed line with red squares), and to 0 K^{-1} (solid line with red squares). The measured $\Delta\lambda(T)$ extracted from Figure 3 is shown for comparison. b) The impact of different cavity lengths when using the measured values of dn/dT for HfO_2 and SiO_2.

cavity length, see Section S4 (Supporting Information) for further discussion.

The fabricated UVB VCSELs with an athermalized lasing wavelength had a short cavity length of 2.5λ to increase the influence of the negative dn/dT of HfO_2 in the DBRs. Figure 4b shows the simulated temperature-induced wavelength shifts for this 2.5λ cavity, but also for larger cavity lengths assuming the same negative dn/dT in the HfO_2. Already for a 5λ cavity length, the influence from the HfO_2 is greatly reduced and the wavelength shift increase with temperature is almost linear, as is observed in most reported III-nitride VCSELs.[7–11]

In general, the simulations are able to predict the measured $\Delta\lambda(T)$ well up to 50 °C, but a discrepancy is observed for temperatures exceeding 50 °C, as shown in Figure 4a. The reason for this can be understood by referring to Figure 2, where it is shown that the measured $\Delta n(T)$ of HfO_2 gradually shifts more slowly for temperatures above 50 °C. However, the measured wavelength shift with temperature in Figure 4a suggests that the negative dn/dT of the HfO_2 used in the VCSEL's DBRs persists up to 80 °C. As the negative dn/dT of HfO_2 is not sufficiently investigated in literature, we can only speculate about the actual reasons. We believe that the discrepancy arises from the different substrates on which the HfO_2 was deposited. The refractive index measurement was performed on a 400-nm-thick HfO_2 layer deposited on a Si substrate, whereas the device DBRs were on AlGaN membranes. Since the thermal expansion coefficient of AlGaN, 4.2–5.7 × 10^{-6} K^{-1},[25,26] is significantly larger than that of Si, 2.6 × 10^{-6} K^{-1},[27] the HfO_2 layers in the devices will have more tensile strain, and potentially a lowered refractive index compared to the ones on Si.[12,17] Another reason could be that in a multilayered stack, as the DBR, annealing of the layers during deposition or processing and built-in strain[12] might influence the exact values of dn/dT.

5. Athermalization of VCSELs with Long Cavity Lengths

Using a short cavity length and a dielectric material with negative dn/dT in the DBR is efficient to athermalize the lasing wavelength of the VCSEL. However, a short cavity leads to a laser with

higher thermal resistance and thus stronger self-heating.[7,9,28,29] This will be an even more pronounced issue in UV-emitting VCSELs due to the poor thermal conductivity of AlGaN compared to GaN, which is used in the cavity of blue VCSELs.[30] The increased operating temperature degrades the device performance in several ways. Heating detunes the gain spectrum with respect to the resonance and reduces the peak gain through a decreased radiative recombination, and an increased non-radiative recombination, carrier leakage and broadening of the carrier distribution. In addition, high temperatures also reduces the device lifetime.

Therefore, to reduce thermal resistance, a longer cavity length should be used. However, when using longer cavities, the penetration depth of the optical field into the DBRs becomes small in comparison with the total cavity length. To achieve an athermalized lasing wavelength, we propose to include a thick dielectric spacer layer in the cavity, having a negative dn/dT. Preferably, this spacer layer should be placed on the top side of the cavity to not impede heat dissipation through the substrate. For an electrically driven VCSEL, current can still be injected in this type of structure through intracavity contacts as are commonly used in III-nitride VCSELs. **Figure 5** shows the wavelength shift as a function of temperature obtained from effective index simulations for different HfO_2 spacer thicknesses added on top of a 10λ AlGaN cavity. As seen, an HfO_2 thickness of 2.5λ produces a temperature stable behavior between 22 and 80 °C. This can also be predicted by the simple expression in Equation (1), that is valid for a long cavity length, namely

$$\frac{d\lambda_{FP}}{dT} = \frac{\lambda_0}{\bar{n}_{c0}}\frac{d\bar{n}_c}{dT} = \frac{\lambda_0}{L_{tot}\bar{n}_{c0}}\left(L_c\frac{dn_c}{dT} + L_s\frac{dn_s}{dT}\right) = 0, \quad (4)$$

where $L_{tot} = L_c + L_s$ is the combined length of the semiconductor cavity, L_c, and the dielectric spacer layer, L_s. From Equation (4), we get for a 10λ AlGaN cavity that the HfO_2 spacer thickness should be

$$L_s = -\frac{dn_c/dT}{dn_s/dT}L_c \approx 2.5\lambda \quad (5)$$

**ADVANCED
SCIENCE NEWS**

www.advancedsciencenews.com

LASER
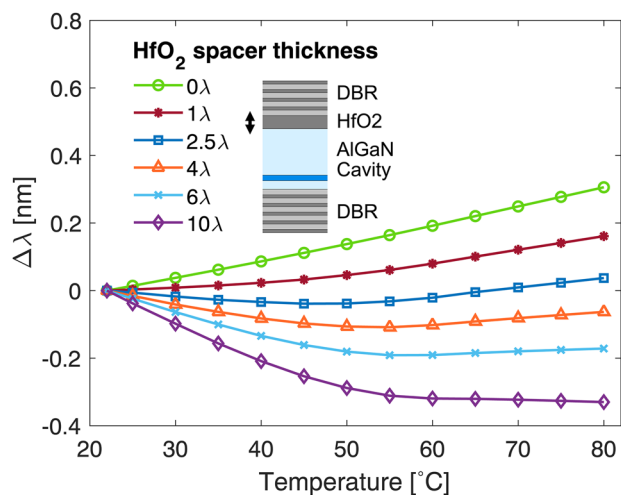& PHOTONICS
REVIEWS

www.lpr-journal.org

Figure 5. Simulated wavelength shift as a function of temperature, $\Delta\lambda(T)$, for a UVB VCSEL with a 10λ cavity length and a HfO$_2$ spacer within the cavity with negative dn/dT.

This simple expression is very effective to design long-cavity length VCSELs with an athermal resonance wavelength. To achieve athermalized VCSELs with good performance over a wide temperature range, the active region should have a small gain peak shift with temperature to minimize the change in detuning over the temperature range of interest. Note that keeping the lasing wavelength fixed can cause an increased detuning between the resonance and gain at higher temperatures, leading to a slightly higher threshold, as discussed in Section S5 (Supporting Information). This approach also works to athermalize electrically driven VCSELs with significant self-heating as discussed in Section S6 (Supporting Information).

6. Conclusion

We have demonstrated a concept for achieving an athermalized lasing wavelength in VCSELs, implemented for an optically pumped UVB VCSEL. The approach is based upon incorporating a material with a negative dn/dT in the DBR to compensate the positive dn/dT of the AlGaN cavity. A short cavity length of 2.5λ was used to ensure a significant overlap between the optical field and the HfO$_2$ layers in the DBRs. This leads to an efficient compensation of the increasing round-trip phase shift with temperature in the AlGaN by the decreasing round-trip phase shift with temperature in the DBRs. The fabricated VCSEL showed a wavelength shift of less than 0.1 nm over a temperature range from 22 °C to 80 °C with a maximum slope of −3.4 pm K^{-1} between 30 and 50 °C. For highly efficient VCSELs, a long cavity length is however required for better heat dissipation. To achieve an athermalized lasing wavelength also in such devices, a HfO$_2$ spacer layer could be added between the AlGaN cavity and the DBR. The concepts proposed and demonstrated here for obtaining a temperature-insensitive lasing wavelength are generic and can be applied to VCSELs in all material systems and with all lasing wavelengths.

7. Experimental Section

Determination of Temperature Dependent Refractive Index: To design and fabricate a VCSEL with an athermal lasing wavelength requires knowledge of the exact dn/dT of all the materials used. For the dielectric materials used in this work, SiO$_2$ and HfO$_2$, temperature-dependent ellipsometry was used to determine dn/dT, and the results are shown in Figure 2 for a wavelength of 310 nm (close to the lasing wavelength of the fabricated VCSELs). The measurements were performed on a 1000-nm-thick SiO$_2$ film and a 400-nm-thick HfO$_2$ film, both deposited on Si. In the temperature range 22–50 °C dn/dT was positive for SiO$_2$, 8.1×10^{-6} K^{-1}, whereas it was negative for HfO$_2$, -2.1×10^{-4} K^{-1}.

To estimate dn/dT of Al$_x$Ga$_{1-x}$N, the measured refractive index data at room temperature[31] was spectrally shifted with the same amount as the measured bandgap, E_g, shifted with temperature. Temperature-dependent photoluminescence (PL) measurements were used to extract $E_g(T)$ for Al contents of $x = 0.2$ (QWs), 0.5 (barriers) and 0.6 (cavity).

The temperature dependent PL measurements were performed using an unprocessed, as-grown UVB VCSEL structure using a frequency-quadrupled Nd:YAG laser laser emitting at 236.5 nm with a repetition rate of 0.5 kHz, a pulse width of 925 ns, and a spot size diameter of 30 μm. Details of the PL measurements are provided in Section S2 (Supporting Information). The resulting change in refractive index as a function of temperature, $\Delta n(T)$, at 310 nm was shown in Figure 2 for the different materials. Refractive index was not only affected by temperature, but also by free-carrier concentration.[32] This effect was estimated using a self-consistent Schrödinger–Poisson k·p formalism using Fermi–Dirac band population[33] and was concluded to be small. More details can be found in Section S4 (Supporting Information).

Device Characterization: To measure the lasing wavelength shift with temperature, the UVB VCSELs were mounted on a heated stage. The VCSELs were optically pumped using a pulsed 266 nm laser with a pulse duration of 0.55 ns and a repetition rate of 20.5 kHz with a pump spot diameter of 30 μm and the VCSEL's emission spectra were analyzed at different stage temperatures using a spectrometer with a resolution of less than 30 pm. The substrate temperature was changed in 2 °C steps.

Supporting Information

Supporting Information is available from the Wiley Online Library or from the author.

Conflict of Interest

The authors declare no conflict of interest

Author Contributions

T.K. developed and grew the pseudosubstrate, and J.E. grew the rest of the epitaxial heterostructures supervised by T.W. and M.K. F.H. developed

the fabrication process and performed the device processing with assistance from J.E. Å.H. and J.C. proposed and supervised the temperature-dependent effective index simulations of the VCSEL structures performed by L.P., which were based on previous work by G.C. L.P. developed the analytical formalism for explaining the results under supervision of Å.H. and J.C. L.P. performed the measurements of the optical spectra as a function of substrate temperature and the temperature-dependent photoluminescence measurements under supervision of J.C. J.C. performed the temperature-dependent ellipsometry measurements. L.P. performed the calculations of the carrier-induced refractive index change based on previous work by J.C. L.P wrote the manuscript with input from the other coauthors.

Data Availability Statement

The data that support the findings of this study are available from the corresponding author upon reasonable request.

Keywords

[1] S. Lin, J. Chang, J. Sun, P. Xu, *Front. Phys.* **2022**, *10*, 853966.
[2] Y. Jiang, A. Ludlow, N. Lemke, R. W. Fox, J. A. Sherman, L.-S. Ma, O. W. Oates, *Nat. Photon* **2011**, *5*, 158.
[3] V. A. Shchukin, N. N. Ledentsov, T. Slight, W. Meredith, N. Y. Gordeev, A. M. Nadtochy, A. S. Payusov, M. V. Maximov, S. A. Blokhin, A. A. Blokhin, Y. M. Zadiranov, N. A. Maleev, V. M. Ustinov, K. D. Choquette, *Proc. SPIE* **2016**, *9766*, 1.
[4] A. Liu, P. Wolf, J. A. Lott, D. Bimberg, *Photon. Res.* **2019**, *7*, 121.
[5] M. Osinski, *Proc. SPIE* **1995**, *2398*, 42.
[6] Y.-C. Chang, L. A. Coldren, in *Design and Performance of High-Speed VCSELs*, Springer, Berlin, Heidelberg **2013**, pp. 233–262.
[7] M. Kuramoto, S. Kobayashi, T. Akagi, K. Tazawa, K. Tanaka, T. Saito, T. Takeuchi, *Appl. Phys. Express* **2018**, *11*, 112101.
[8] T.-C. Chang, S.-Y. Kuo, J.-T. Lian, K.-B. Hong, S.-C. Wang, T.-C. Lu, *Appl. Phys. Express* **2017**, *10*, 112101.
[9] Y. Mei, R.-B. Xu, H. Xu, L.-Y. Ying, Z.-W. Zheng, B.-P. Zhang, M. Li, J. Zhang, *Semicond. Sci. Technol.* **2018**, *33*, 015016.
[10] T.-C. Lu, T.-T. W. Wu, S.-W. Chen, P.-M. Tu, Z.-Y. Li, C.-K. Chen, C.-H. Chen, H.-C. Kuo, S.-C. Wang, H.-W. Zan, C.-Y. Chang, *IEEE J. Sel. Top. Quantum Electron.* **2011**, *17*, 1594.
[11] C. O. Holder, J. T. Leonard, R. M. Farrell, D. A. Cohen, B. Yonkee, J. S. Speck, S. P. DenBaars, S. Nakamura, *Appl. Phys. Lett.* **2014**, *105*, 031111.
[12] J. Bovington, R. Wu, K.-T. Cheng, J. E. Bowers, *Opt. Express* **2014**, *22*, 661.
[13] S. S. Djordjevic, K. Shang, B. Guan, S. T. S. Cheung, L. Liao, J. Basak, H.-F. Liu, S. J. B. Yoo, *Opt. Express* **2013**, *21*, 13958.
[14] F. Qiu, A. M. Spring, F. Yu, S. Yokoyama, *Appl. Phys. Lett.* **2013**, *102*, 051106.
[15] O. Reshef, K. Shtyrkova, M. G. Moebius, S. Griesse-Nascimento, S. Spector, C. C. Evans, E. Ippen, E. Mazur, *JOSA B.* **2015**, *32*, 2288.
[16] S. Feng, K. Shang, J. T. Bovington, R. Wu, K.-T. Cheng, J. E. Bowers, S. J. B. Yoo, *Proc. IEEE IPC* **2014**, 116.
[17] L. Prod'Homme, *Phys. Chem. Glasses.* **2014**, *1*, 119.
[18] S. Wiechmann, J. Müller, *Thin Solid Films* **2009**, *517*, 6847.
[19] G. Gülşen, M. Naci Inci, *Opt. Mater.* **2002**, *18*, 373.
[20] F. Hjort, J. Enslin, M. Cobet, M. A. Bergmann, J. Gustavsson, T. Kolbe, A. Knauer, F. Nippert, I. Häusler, M. R. Wagner, T. Wernicke, M. Kneissl, Å. Haglund, *ACS Photonics* **2021**, *8*, 135.
[21] D. I. Babic, S. W. Corzine, *IEEE J. Quantum Electron.* **1992**, *28*, 514.
[22] M. A. Bergmann, J. Enslin, F. Hjort, T. Wernicke, M. Kneissl, Å. Haglund, *Appl. Phys. Lett.* **2020**, *116*, 121101.
[23] G. Cardinali, F. Hjort, N. Propkop, J. Enslin, M. Cobet, M. A. Bergmann, J. Gustavsson, J. Ciers, I. Häusler, T. Wernicke, Å. Haglund, M. Kneissl, *Appl. Phys. Lett.* **2022**, *121*, 103501.
[24] G. R. Hadley, *Opt. Lett.* **1995**, *20*, 1483.
[25] C. Roger, S. Einfeldt, S. Figge, D. Hommel, *Phys. Rev. B.* **2005**, *72*, 085218.
[26] W. M. Yim, R. J. Paff, *J. Appl. Phys.* **1974**, *45*, 1456.
[27] H. Watanabe, N. Yamada, M. Okaju, *Int. J. Thermophys.* **2003**, *25*, 221.
[28] R. P. Sarzała, P. Śpiewak, M. Wasiak, *IEEE J. Quantum Electron.* **2019**, *55*, 1.
[29] S. Mishkat-Ul-Masabih, J. Leonard, D. Cohen, S. Nakamura, D. Feezell, *Phys. Status Solidi A* **2017**, *214*, 1.
[30] W. Liu, A. A. Balandin, *J. Appl. Phys.* **2017**, *97*, 073710.
[31] M. Winkler, *Otto von Guericke University Magdeburg* **2017**, Unpublished raw data.
[32] U. T. Schwarz, E. Sturm, W. Wegscheider, V. Kümmler, A. Lell, V. Härle, *Appl. Phys. Lett.* **2003**, *83*, 4095.
[33] J. Ciers, G. Jacopin, G. Callsen, C. Bougerol, J.-F. Carlin, R. Butté, N. Grandjean, *Jpn. J. Appl. Phys.* **2018**, *57*, 090305.